Mammalian lipid droplets are innate immune hubs integrating cell metabolism and host defense

Marta Bosch, Miguel Sánchez-Álvarez, Alba Fajardo, Ronan Kapetanovic, Bernhard Steiner, Filipe Dutra, Luciana Moreira, Juan Antonio López, Rocío Campo, Montserrat Marí, et al.

▶ **To cite this version:**

Marta Bosch, Miguel Sánchez-Álvarez, Alba Fajardo, Ronan Kapetanovic, Bernhard Steiner, et al.. Mammalian lipid droplets are innate immune hubs integrating cell metabolism and host defense. Science, 2020, 370 (6514), pp.eaay8085. 10.1126/science.aay8085 . hal-04337099

HAL Id: hal-04337099
https://hal.inrae.fr/hal-04337099

Submitted on 12 Dec 2023

HAL is a multi-disciplinary open access archive for the deposit and dissemination of scientific research documents, whether they are published or not. The documents may come from teaching and research institutions in France or abroad, or from public or private research centers.

L'archive ouverte pluridisciplinaire **HAL**, est destinée au dépôt et à la diffusion de documents scientifiques de niveau recherche, publiés ou non, émanant des établissements d'enseignement et de recherche français ou étrangers, des laboratoires publics ou privés.

Mammalian lipid droplets are innate immune hubs integrating cell metabolism and host defense

Marta Bosch [1, 2, *, †], Miguel Sánchez-Álvarez [3, †], Alba Fajardo [1], Ronan Kapetanovic [4, 5, 6], Bernhard Steiner [4], Filipe Dutra [7], Luciana Moreira [7], Juan Antonio López [8, 9], Rocío Campo [8], Montserrat Marí [11], Frederic Morales-Paytuví [1], Olivia Tort [1], Albert Gubern [1], Rachel M. Templin [4, 10], James E. B. Curson [4, 5, 6], Nick Martel [4], Cristina Català [12], Francisco Lozano [2, 12], Francesc Tebar [1, 2], Carlos Enrich [1, 2], Jesús Vázquez [8, 9], Miguel A. Del Pozo [3], Matthew J. Sweet [4, 5, 6], Patricia T. Bozza [7], Steven P. Gross [13], Robert G. Parton [4, 10, *] and Albert Pol [1, 2, 14, *].

[1] Cell compartments and Signaling Group, Institut d'Investigacions Biomèdiques August Pi i Sunyer (IDIBAPS) and [2] Department of Biomedical Sciences, Faculty of Medicine, Universitat de Barcelona. 08036, Barcelona.
[3] Mechanoadaptation and Caveolae Biology Laboratory, Cell and Developmental Biology Area, Centro Nacional de Investigaciones Cardiovasculares (CNIC). 28029, Madrid, Spain.
[4] Institute for Molecular Bioscience (IMB) and [5] IMB Centre for Inflammation and Disease Research, [6] Australian Infectious Diseases Research Centre, The University of Queensland (UQ), Brisbane, Queensland 4072, Australia.
[7] Laboratório de Imunofarmacologia, Instituto Oswaldo Cruz, FIOCRUZ, Rio de Janeiro, RJ, CEP 21.040-900, Brazil.
[8] Cardiovascular Proteomics Laboratory, Vascular Pathophysiology Area, CNIC and [9] CIBER-CV, Instituto de Salud Carlos III. 28029, Madrid, Spain.
[10] Centre for Microscopy and Microanalysis, UQ.
[11] Department of Cell Death and Proliferation, Institut d'Investigacions Biomèdiques de Barcelona (IIBB-CSIC) and IDIBAPS.
[12] Immunoreceptors of the Innate and Adaptive System team, IDIBAPS.
[13] Department of Developmental and Cell Biology, UC Irvine, Irvine, Ca 92697, USA.
[14] Institució Catalana de Recerca i Estudis Avançats (ICREA), 08010, Barcelona.

[†] These two authors made equal contribution to this work.
[*] To whom correspondence should be addressed: martabosch@ub.edu, r.parton@imb.uq.edu.au, or apols@ub.edu.
M.B.: Centre de Recerca Biomèdica CELLEX (IDIBAPS), Lab 1B, Casanova 143, 08036 Barcelona. Ph.: (34) 932275400 ext 3358.
R.G.P.: Institute for Molecular Bioscience, University of Queensland, Queensland 4072, Brisbane, Australia. Ph.: (61) 733462032.
A.P.: Centre de Recerca Biomèdica CELLEX (IDIBAPS), Office B12, Casanova 143, 08036 Barcelona. Ph.: (34) 932275400 ext 3337.

Short title: Lipid droplets are innate immune hubs.
Key words: Lipid droplets, mitochondria, innate immunity, immunometabolism, proteomics, antibiotics, cathelicidin.

Abstract

Lipid droplets (LDs) are the major lipid storage organelles of eukaryotic cells and a source of nutrients for intracellular pathogens. Here, we demonstrate that mammalian LDs are endowed with a protein-mediated antimicrobial capacity, which is upregulated by danger signals. In response to lipopolysaccharide (LPS), multiple host defense proteins, including interferon-inducible GTPases and the antimicrobial cathelicidin, assemble into complex clusters on LDs. LPS additionally promotes the physical and functional uncoupling of LDs from mitochondria, reducing fatty acid metabolism while increasing LD-bacterial contacts. Thus, LDs actively participate at two levels of mammalian innate immunity: first, they are cell-autonomous organelles that organize and utilize immune proteins to kill intracellular pathogens; and second, they are central players in the local and systemic metabolic adaptation to infection.

Lipid droplets (LDs) are the major lipid storage organelles of eukaryotic cells (*1*). Common parasites (e.g. trypanosomes and *Plasmodium falciparum*), bacteria (e.g. mycobacteria and *Chlamydia*), and viruses (e.g. hepatitis C (HCV) and dengue (DENV)) induce and target LDs during their life cycles (*2*). The current view is that LDs support infection, providing invaders with substrates for survival and/or growth (*3*). However, successful innate defense is critical for survival and host immune responses have co-evolved with pathogens developing a plethora of defense mechanisms. Indeed, there is some limited evidence that LDs actively participate in innate defense (*4, 5*). For example, three innate immunity-related proteins localize to LDs of infected cells: (i) viperin, active against two viruses assembled on LDs (HCV and DENV) (*6*); (ii) the IFN-γ-inducible GTPase (IGTP), required for resistance to *Toxoplasma gondii (7);* and (iii) histones on LD, which increase survival of bacterially challenged *Drosophila* embryos (*8*). Here, we analyzed whether mammalian LDs have a direct or regulated role in immune defense. Since all eukaryotic cells accumulate LDs, this innate defense mechanism may be ubiquitous and therefore serve as a suitable target for therapeutic intervention.

Results

Mammalian LDs display regulated protein-mediated antibacterial activity

We selected hepatic LDs as a proof of concept that mammalian LDs participate in innate immunity. The liver modulates the systemic immune response and hepatic LDs are targeted by LD-related pathogens (*9*). We tested the antibacterial capacity of hepatic LD proteins in a bacterial killing assay of *Escherichia coli*, an abundant component of the intestinal microbiota and cause of serious clinical infections. First, we injected mice with lipopolysaccharide (LPS), an activator of innate immunity (*10*). Since LPS-treated animals (LPS-mice) reduce food intake, LPS-mice were additionally fasted and compared to mice

injected with saline buffer and identically fasted (CTL-mice). Both treatments promoted similar levels of hepatic triglycerides (Fig. 1, A and B; and Fig. 1C), although morphological differences between LDs were evident by electron microscopy (TEM). The number of LDs in LPS-treated livers (LPS-LDs) was higher than in fasted animals (CTL-LDs) although LPS-LDs were smaller (Fig. 1, D and E). CTL- and LPS-LDs were purified (Fig. 1F; and fig. S1A) and LD proteins incubated with *E. coli*. Bacterial viability was estimated from the resulting colony-forming units (CFU) (Fig. 1G; and fig. S1B). LD proteins reduced bacterial growth and LPS-LD proteins demonstrated enhanced antibacterial capacity (Fig. 1G). This enhancement was confirmed in suspension cultures (fig. S1C) and using LD proteins from fed mice (fig. S1, D and E). To determine LD antibacterial activity during an actual infection, mouse liver LDs were obtained after cecal ligation and puncture (CLP), a model of polymicrobial sepsis. CLP-LD proteins exhibited enhanced antibacterial capacity when compared to CTL-LDs (fig. S1, B and F). LPS- and CLP-LD proteins reduced bacterial growth even after a shorter incubation time (fig. S1, G and H). Bacterial growth was unaffected by oleic acid (OA), the major fatty acid component of hepatic LDs, or by cytosolic proteins from CTL- and LPS-livers (fig. S1, I and J). Thus, mammalian LDs have a protein-mediated antibacterial capacity, which is regulated by infection.

Next, we analyzed whether LDs reduce bacterial growth in human monocyte-derived macrophages from healthy donors (HMDMs). In HMDMs, LD accumulation was promoted by incubation with OA, a fatty acid efficiently esterified into LDs (*11*). Untreated and LD-loaded HMDMs were infected with either non-pathogenic *E. coli* or the professional intramacrophage pathogen *Salmonella enterica* serovar Typhimurium (*Salm*). HMDMs responded to infection by increasing LD numbers (Fig. 1H). *E. coli* survival (Fig. 1I), but not phagocytic capacity (Fig. 1K), was reduced in LD-loaded HMDMs. By contrast, LDs did not

reduce *Salm* survival (Fig. 1J), in keeping with this pathogen's ability to avoid antimicrobial responses (*12*). In *E. coli*-infected macrophages, LDs were often in the proximity of bacteria (Fig. 1, M to R). Comparative analyses demonstrated that LDs were closer to and more frequently established longer contacts with *E. coli* than with *Salm* (Fig. 1L; and fig. S2, A and B). These LD-*E. coli* contact sites increased in loaded HMDMs (fig. S2, C and D). TEM analysis revealed that in LD-*E. coli* contact sites, the LD monolayer (containing LD proteins) produced an apparent discontinuity in the bacterial vacuolar membrane and probably interacted with the bacterial periplasm (Fig. 1, O to R; and fig. S2, E and F). Thus, LD-loaded macrophages display enhanced antibacterial capacity, which suggests the existence of docking mechanisms that enable or facilitate the engagement of antibacterial LD proteins with bacteria.

Quantitative mass spectrometry analysis of LPS-LDs

To characterize the enhanced LPS-LD antibacterial capacity, we performed comparative mass spectrometry profiling of proteins differentially associated with LPS- or CTL-LDs (*13*). CTL- and LPS-livers were analyzed in parallel. Stringent analysis (FDR<1) of LPS-livers identified 8563 proteins of which 1136 (cut-off $|\Delta Zq| \geq 1.8$) were differentially expressed (553 enriched/583 reduced) (Fig. 2A; table S1; and table S2). In LPS-LDs, 3392 proteins were identified (table S3), of which 689 were differentially distributed (317 enriched/372 reduced) (table S4; and table S5). Only 8% of the enriched and 0.8% of the downregulated proteins in LPS-LDs followed an equivalent profile in LPS-livers (Fig. 2A; Fig. 2B; and fig S3A), indicating autonomous changes in LPS-LDs. Functional annotation enrichment analysis revealed the upregulation of proteins related to the acute phase and inflammatory responses and significant reduction of mitochondrial proteins co-fractionating with LDs (Fig. 2B; and fig S2A).

Published proteomic analyses showed that approximately 7-10% of proteins in LD fractions are bona fide LD resident proteins (*14, 15*), reflecting the tight interaction of LDs with other organelles. Of 3392 identified proteins in LPS-LDs, 238 (7%) were annotated as LD-resident proteins by the Ingenuity Pathway Analysis (IPA) platform or by at least one of the above proteomic analyses (Fig. 2C; and table S6). Seventy-two of these LD proteins were LPS-regulated (59 enriched/13 reduced) (table S7). Thus, 30% of the identified LD proteome, including the five perilipins (PLINs), was LPS-sensitive. PLIN2 (ΔZq=6.47) and RAB18 (ΔZq=7.10) were highly enriched and PLIN5 was the only downregulated PLIN (ΔZq=minus 4.13) (table S7). Two immune proteins previously described on LDs, viperin (RSAD2, ΔZq=8.12) and IGTP (IRGM3, ΔZq=6.7), were identified on LPS-LDs, validating our proteomic strategy (table S4). IPA analysis of these LD resident proteins demonstrated enrichment of innate immunity-related components and reduction of metabolism-related LD resident proteins (fig. S3B).

To identify relevant candidates on LPS-LDs, we initially performed hierarchical clustering of proteins with similar variation profiles across each individual replicate, likely reflecting co-regulation (Fig. 2D). Gene interaction analysis of correlated proteins revealed the existence of several functionally connected clusters such as clusters of RAB GTPases, a cluster containing PLIN1 and histones, and a network of metabolism regulators including PLIN3, PNPLA2 (ATGL), and ACSL4 (fig. S4A). Notably, the cluster containing proteins ranking highest for enrichment (ΔZq>3.14) nucleated around PLIN2 and included viperin, IGTP, and several immune GTPases (GVIN, IFGGA1, IFGGB55, IFI47, and IFI35) (Fig. 2D). These functionally related proteins may also physically interact. We confirmed that PLIN2 interacts with IGTP (*7*) and detected a weak interaction with cathelicidin (fig. S4B). Finally, we

performed a gene interaction analysis across the whole LPS-sensitive LD proteome (ΔZq>1.8). The analysis retrieved complex protein networks (Fig. 2E) suggesting that LDs are innate immune hubs integrating major intra- and extracellular responses.

We validated the proteomic data by immunoblotting and confirmed enrichment of PLIN2 and PLIN3 on LPS-LDs in contrast with the unregulated lipase HSL (ΔZq=0.04) (Fig. 3A). PLIN2 expression was further confirmed in mouse liver sections (fig. S5A). PLIN2 in LPS- and CLP-livers was predominantly expressed in hepatocytes around periportal regions where cells receive blood and regulatory inflammatory mediators. Direct transcriptional regulation of LD proteins by inflammatory stimuli was assessed in human hepatic HuH7 cells treated with LPS, TNF, or IFN-γ (fig. S5 B) *PLIN2* and *PLIN5* expression was differentially regulated by individual cytokines (fig. S5C). Thus, LPS likely regulates LD protein composition directly and in conjunction with paracrine signaling networks.

Physical and functional uncoupling of LPS-LDs and mitochondria

Mitochondria are key organelles for innate immunity (*16*). During nutrient starvation, LDs contact mitochondria to supply fatty acids fueling oxidative phosphorylation (OXPHOS) (*17*). By contrast, challenged innate immune cells increase aerobic glycolysis and reduce OXPHOS (*16*). Therefore, uncoupling LPS-LDs and mitochondria (Fig. 2B) may contribute to a reduction of OXPHOS in infected cells. Reduced interaction between LPS-LDs and mitochondria was confirmed by decreased co-fractionation of ATP5D (a subunit of ATP synthase, an OXPHOS enzyme) when compared to CTL-LDs (Fig. 3, A and B). Functional annotation of reduced mitochondrial proteins co-fractionating with LPS-LDs matched with the whole mitochondrial proteome (MitoCarta 2.0) (Fig. 3, C). This does not reflect a reduced mitochondrial content of LPS-livers as determined by: (i) functional annotation enrichment

analysis; (ii) citrate synthase activity; and (iii) cytochrome oxidase (*COI*) gene copy number (Fig. 3, D and E). Further, the reduced number of contacts between LPS-LDs and mitochondria was confirmed by TEM (Fig. 3F; and fig. S6, A and B). In these images, ER membranes often separated LPS-LDs and mitochondria (fig. S6C). Finally, we confirmed two functional consequences of uncoupling: (i) reduced mitochondrial beta-oxidation of lipids supplied by LDs in LPS-primary hepatocytes (Fig. 3, G and H); and (ii) lower levels of circulating ketones in LPS-mice serum (Fig. 3I). These results extend and mechanistically explain early observations showing reduced beta-oxidation and ketogenesis in rats infected with *Streptococcus pneumoniae*, *Francisella tularensis*, and *S.* Typhimurium *(18)*.

PLIN5 tethers LDs and mitochondria (*17*). Interestingly, PLIN5 is the only perilipin downregulated in LPS-LDs. During fasting, to facilitate LD-mitochondria contacts, PLIN5 levels increase on hepatic LDs (Fig. 3J). However, PLIN5 levels on LDs were reduced when fasted mice were treated with LPS (Fig. 3, A and J). Further, human *PLIN5* expression promoted co-clustering of LDs and mitochondria in HuH7 cells (Fig. 3K). To explore the role of PLIN5, *PLIN5* was transfected in LPS-responsive HEK293-TLR4^{+} cells (fig. S7, A to C) and the LD-mitochondrial contacts quantified. *PLIN5* expression increased the number and length of these contacts (Fig. 3L; and fig. S7, D to F). In LPS-treated HEK293-TLR4^{+} cells, the overall length of the contacts was reduced in CTL- but not in *PLIN5*-expressing cells (Fig. 3L). In *PLIN5*-expressing cells, LPS only modestly reduced the total number of contacts (fig. S7E) and increased the average length of remaining contacts (fig. S7F). Thus, LPS directly regulates dynamics of LD-mitochondrial contacts. Furthermore, PLIN5 downregulation appears to be involved in the LPS-induced metabolic reprogramming.

We next evaluated the role of PLIN5 in other aspects of immune defense. *PLIN5*-overexpressing HEK293 cells exhibited a significantly reduced capacity to clear *E. coli* by comparison to *PLIN3*-overexpressing control cells (Fig. 3M). Furthermore, THP-1 cells lentivirally transduced with *PLIN5*, and subsequently infected with *E. coli*, exhibited impaired antimicrobial capacity (Fig. 3N), increased numbers of LD-mitochondria contacts (fig. S7, G to I), and reduced LD-bacteria interactions (fig. S7J). Thus, LPS-mediated PLIN5 downregulation reduces LD-mitochondrial tethering, enabling an effective antimicrobial response.

LDs accumulate and utilize innate immunity proteins

Our proteomic analyses predicted complex immune protein networks on LDs (Fig. 2D, and fig. S4A). Given that many known antipathogenic proteins were associated with the PLIN2 cluster (Fig. 2D), we next assessed components of this cluster for LD association. The antiparasitic protein IGTP, the antiviral protein viperin as well as three GTPases (IIGP1, TGTP1, and IFI47) were all shown to associate with LDs (Fig. 4, A to C; fig. S8; and fig. S9). Thus, multiple proteins associated with responses to different classes of pathogens localize to LDs. The PLIN2 cluster also includes cathelicidin (CAMP, ΔZq=7.25), a broad-spectrum antimicrobial peptide with chemotactic and immunomodulatory properties (*19*). Cathelicidins are synthesized as proproteins that, after cleaving a N-terminal signal peptide, follow the exocytic pathway (Fig. S10A). The presence of CAMP on LDs is unknown.

We confirmed the accumulation of CAMP on LPS-LDs (Fig. 4A) and the distribution of a human-tagged CAMP between the ER and LDs of HuH7 cells (Fig. 4B; and fig. S10, B to D). CAMP on LDs had a higher molecular weight than CAMP in the ER (Fig. 4C; and fig. S10E), suggesting that the CAMP hydrophobic domain functions as both, as a signal peptide

cleaved for secretion via the ER but also as an uncleaved LD-targeting signal. Such dual distribution occurs for other LD proteins containing signal peptides, such as apolipoproteins (*20*). Indeed, the low-molecular-weight (20 kDa) CAMP species corresponded to the protein with a cleaved signal peptide following the secretory pathway (fig. S10, F to H). Distribution of overexpressed CAMP, as well as other immune LD proteins, was not directly affected by LPS-TLR4 signaling (fig. S11), indicating that LPS does not directly regulate the intracellular trafficking of these proteins.

We next investigated the role of CAMP in HMDMs. Silencing of *CAMP* (Fig. 4D) impaired the antibacterial response of the macrophages against *E. coli* (Fig. 4E). Furthermore, although LD-loading significantly reduced bacterial survival, this treatment regime was unable to do so in CAMP-silenced HMDMs. Thus, the antibacterial activity of LDs in HMDMs appears to require CAMP. To further explore this possibility, a LD-resident CAMP was engineered by substitution of the CAMP signal peptide with the ALDI LD-targeting motif (fig. S12; A and B) (*21*). Modified CAMP (LD-CAMP) accumulated on LDs of HuH7 cells (fig. S12, C to F) and showed a single electrophoretic mobility pattern, matching the higher molecular weight CAMP that localized to LDs (Fig. 4C; and fig. S12C). Next, HEK293 cells were transfected with LD-*CAMP* and protein distribution on LDs confirmed with anti-CAMP antibodies (Fig. 4F), demonstrating a native conformation. The antimicrobial capacity of LD-CAMP was then assessed. Bacterial loads of *E. coli*, methicillin-resistant *Staphylococcus aureus* (MRSA), and *Listeria monocytogenes* were significantly reduced in LD-*CAMP* expressing cells when compared to those expressing the *PLIN3* control (Fig. 4G). By contrast, *Pseudomonas aeruginosa* loads were not affected by LD-*CAMP*, suggesting that this pathogen subverts this innate defense response. The impact of LD-*CAMP* overexpression on bacterial survival was dependent on LD formation (Fig. 4, H to J). The tagged LD-*CAMP* demonstrated a similar

antibacterial activity to wild-type *CAMP* and a slightly augmented stability when compared to an untagged LD-*CAMP* (fig. S12, G to J). Therefore, LDs act as a molecular switch in innate immunity, responding to danger signals by both reprogramming cell metabolism and eliciting protein-mediated antimicrobial defense.

Discussion

Pathogens require host-derived lipids to support their life cycles, with LDs providing a source of these lipids (*22*). As a result, LDs also have the potential to deliver effective host defenses against intracellular pathogens. We show that at least 30% of the LD proteome is LPS-sensitive, suggesting that innate immunity has developed a host defense program that includes extensive LD remodeling. Our analyses demonstrate that complex clusters of immunity-related proteins organize on LDs of infected cells. In addition to previously described LD-resident immune proteins, such as viperin and IGTP, we have identified IIGP1, TGTP1, and IFI47. Our analysis also identified CAMP as a professional antibacterial protein efficiently functioning on LDs. These proteins may act individually, coordinately, and/or synergistically to kill pathogens.

Mechanisms of LD trafficking and docking with phagocytic and parasitophorous membranes, observed here and described for several pathogens (*23-26*), may facilitate the delivery of immune proteins located on the LD surface. Accumulation on LDs may provide stability to these proteins, and may restrict these potentially cytotoxic peptides to LDs preventing indiscriminate cellular damage (*27*). In this respect, we have shown that LPS triggers physical separation of LDs and mitochondria, at least partly due to reduced PLIN5 levels on LPS-LDs (*28*). Uncoupling likely reflects both a self-protection program (to avoid mitochondrial damage, in view of their prokaryotic evolutionary origin), and a means to

maximize or increase the number of LDs available to interact with bacteria. Simultaneously, the reduced LD-mitochondria interaction may lead to distinctive immunometabolism features: (i) accumulation of host LDs resulting from reduced mitochondrial-mediated LD consumption; (ii) reduced OXPHOS displayed by infected cells due to decreased fatty acid oxidation; and (iii) the low rates of ketogenesis displayed by infected animals.

In summary, these studies highlight that mammalian LDs comprise an initial intracellular line of defense. LDs actively participate in at least two levels of the innate response, accumulating and utilizing antibacterial proteins, as well as regulating immune cell metabolism. Since widespread resistance to current antibiotics is common among pathogens, further understanding the cellular mechanisms eliciting LD-mediated defense may provide new strategies for anti-infective development (*29, 30*).

Materials and methods summary

Animals

Detailed information about protocols, instrumentation, and reagents is included in Supplemental Material and Methods. Briefly, C57BL/6J male mice were from Charles River Laboratories (Wilmington, MA, US). Animals were kept under a controlled humidity and lighting schedule with a 12 hours dark period. Food and water were available ad libitum. All animals received humane care in compliance with institutional guidelines regulated by the European Community. Protocols were approved by the Animal Care Committee of the University of Barcelona.

Purification of hepatic LDs

Mice were intraperitoneally injected with saline buffer (CTL-LDs) or with 6 mg/kg of LPS (Sigma-Aldrich, St Louis, MO, US) (LPS-LDs) and fasted overnight. The liver was extracted, and gently homogenized. Hepatic LDs were purified by fractionation in sucrose density gradients. LD proteins were precipitated with acetone, extensively washed, resuspended in Tris buffer, and stored at minus 20ºC before use. In some experiments, mice were identically treated but food and water were available ad libitum (fed-LDs). To purify CLP-LDs, the mouse cecum was exposed, ligated below the ileocecal junction, and punctured three times to induce severe sepsis. Hepatic LD proteins were purified 24 hours later. Sham-operated animals (CTL-LDs) underwent an identical laparotomy but without CLP.

Cell culture

To generate human monocyte-derived macrophages (HMDMs), $CD14^{+ve}$ monocytes were isolated from anonymized human buffy coats obtained from the Australian Red Cross Blood Service. The human monocytic THP-1 cell line was obtained from the American Type Culture Collection (Rockville, MD, US). Human hepatic (HuH7, RRID: CVCL_0336) and human embryonic kidney cells (HEK293, CVCL_0045; ATCC, Manassas, VA) were used in experiments requiring plasmid transfection. HEK293 stably expressing the Toll-like receptor 4 ($HEK293\text{-}TLR4^{+}$) were used to assess the effect of LPS on LDs. Primary hepatocytes were isolated from mice liver by collagenase perfusion and used to determine the impact of LPS on hepatic lipid metabolism.

Bacterial strains

HMDMs were infected with *Salmonella Typhimurium* SL1344 and *Escherichia coli* K-12 MG1655. Heat-killed pHrodoTM Green *E. coli* BioParticlesTM Conjugate (#P35366,

ThermoFisher Scientific) and *E. coli* strain MG1655 or *Salmonella* SL1344 strain, both expressing mCherry, were respectively used to analyze phagocytosis or LD-bacteria proximity in HMDMs. THP-1 cells were lentivirally transduced with *PLIN5* and infected with *E. coli* K-12 MG1655. HEK293 were transfected with LD-*CAMP* using GENEJET PLUS (SignaGen, Rockville, MD, US) and infected with *E. coli* (ATCC 25922), MRSA (Methicillin-resistant *Staphylococcus aureus*, strain 162057-900), *Pseudomonas aeruginosa* (ATCC 27853) and *Listeria monocytogenes* (strain 10403S).

Proteomics

TMT-labeled, fractionated tryptic LD or homogenate peptides were analyzed in an Orbitrap Fusion mass spectrometer and identified on SEQUEST-HT (ThermoFisher, Waltham, MA, US; UniprotKB). Relative protein abundance for ranking and hierarchical clustering is in *Zq* values. Functional annotation and network analyses used IPA DB data (QIAGEN, Hilden, Germany).

Figure preparation

Figures were created using Microsoft PowerPoint (Microsoft 365 MSO). Images were edited with Adobe Photoshop CS3 software (Adobe Systems Inc.). GraphPad Prism 7 (GraphPad Software) was used to create graphs and calculate statistical significances.

Supplementary Materials

Materials and Methods

Figs. S1 to S12

Tables S1 to S7

References (*31-49*)

References and Notes

1. A. Pol, S. P. Gross, R. G. Parton, *J Cell Biol* **204**, 635 (Mar 03, 2014).
2. A. L. Vallochi, L. Teixeira, K. D. S. Oliveira, C. M. Maya-Monteiro, P. T. Bozza, *Front Immunol* **9**, 1022 (2018).
3. P. Roingeard, R. C. Melo, *Cell Microbiol* **19** (Jan, 2017).
4. M. Knight, J. Braverman, K. Asfaha, K. Gronert, S. Stanley, *PLoS Pathog* **14**, e1006874 (Jan, 2018).
5. R. C. Melo, A. M. Dvorak, *PLoS Pathog* **8**, e1002729 (2012).
6. E. R. Hinson, P. Cresswell, *Proc Natl Acad Sci U S A* **106**, 20452 (Dec 01, 2009).
7. L. Bougneres *et al.*, *Immunity* **31**, 232 (Aug 21, 2009).
8. P. Anand *et al.*, *Elife* **1**, e00003 (Nov 13, 2012).
9. U. Protzer, M. K. Maini, P. A. Knolle, *Nat Rev Immunol* **12**, 201 (Feb 24, 2012).
10. J. C. Kagan, *Trends Immunol* **38**, 696 (Oct, 2017).
11. A. Herms *et al.*, *Nat Commun* **6**, 7176 (May 27, 2015).
12. J. Behnsen, A. Perez-Lopez, S. P. Nuccio, M. Raffatellu, *Trends Immunol* **36**, 112 (Feb, 2015).
13. P. Navarro *et al.*, *J Proteome Res* **13**, 1234 (Mar 7, 2014).
14. N. Krahmer *et al.*, *Mol Cell Proteomics* **12**, 1115 (May, 2013).
15. K. Bersuker *et al.*, *Dev Cell* **44**, 97 (Jan 8, 2018).
16. E. L. Mills, B. Kelly, L. A. J. O'Neill, *Nat Immunol* **18**, 488 (Apr 18, 2017).
17. M. Bosch, R. G. Parton, A. Pol, *Semin Cell Dev Biol* (Mar 4, 2020).
18. H. A. Neufeld, J. A. Pace, F. E. White, *Metabolism* **25**, 877 (Aug, 1976).
19. A. Fabisiak, N. Murawska, J. Fichna, *Pharmacol Rep* **68**, 802 (Aug, 2016).
20. X. Shu, L. Nelbach, R. O. Ryan, T. M. Forte, *Biochim Biophys Acta* **1801**, 605 (May, 2010).
21. S. Turro *et al.*, *Traffic* **7**, 1254 (Sep, 2006).
22. C. L. Libbing, A. R. McDevitt, R. P. Azcueta, A. Ahila, M. Mulye, *Cells* **8** (Apr 15, 2019).
23. J. L. Cocchiaro, Y. Kumar, E. R. Fischer, T. Hackstadt, R. H. Valdivia, *Proc Natl Acad Sci U S A* **105**, 9379 (Jul 8, 2008).
24. P. Peyron *et al.*, *PLoS Pathog* **4**, e1000204 (Nov, 2008).
25. K. A. Mattos *et al.*, *Cell Microbiol* **13**, 259 (Feb, 2011).
26. S. J. Nolan, J. D. Romano, I. Coppens, *PLoS Pathog* **13**, e1006362 (Jun, 2017).
27. J. S. Mader, N. Mookherjee, R. E. Hancock, R. C. Bleackley, *Mol Cancer Res* **7**, 689 (May, 2009).
28. S. N. Keenan *et al.*, *Diabetes* **68**, 543 (Mar, 2019).
29. D. J. Greenwood *et al.*, *Science* **364**, 1279 (Jun 28, 2019).
30. R. Dubey *et al.*, *Nat Chem Biol* **16**, 206 (Feb, 2020).
31. D. M. Moujalled *et al.*, *Cell Death Dis* **4**, e465 (Jan 17, 2013).
32. J. M. Murphy *et al.*, *Immunity* **39**, 443 (Sep 19, 2013).
33. M. Bosch *et al.*, *Am J Pathol* **186**, 517 (Mar, 2016).
34. A. Tutusaus *et al.*, *Cell Mol Gastroenterol Hepatol* **9**, 349 (2020).
35. R. Kapetanovic *et al.*, *FASEB J* **30**, 1901 (May, 2016).
36. A. Barrientos, *Methods* **26**, 307 (Apr, 2002).
37. M. Bosch *et al.*, *Curr Biol* **21**, 681 (Apr 26, 2011).
38. C. J. Stocks *et al.*, *J Leukoc Biol* (May 22, 2020).
39. S. Lauer, Y. A. Kunde, T. A. Apodaca, B. Goldstein, E. Hong-Geller, *Cell Immunol* **255**, 8 (2009).
40. A. Kassan *et al.*, *J Cell Biol* **203**, 985 (Dec 23, 2013).

41. A. Pol, D. Ortega, C. Enrich, *Biochem J* **323 (Pt 2)**, 435 (Apr 15, 1997).
42. A. Herms *et al.*, *Curr Biol* **23**, 1489 (Aug 5, 2013).
43. J. R. Kremer, D. N. Mastronarde, J. R. McIntosh, *J Struct Biol* **116**, 71 (Jan-Feb, 1996).
44. J. Schindelin *et al.*, *Nat Methods* **9**, 676 (Jun 28, 2012).
45. C. A. Schneider, W. S. Rasband, K. W. Eliceiri, *Nat Methods* **9**, 671 (Jul, 2012).
46. I. Arganda-Carreras *et al.*, *Bioinformatics* **33**, 2424 (Aug 1, 2017).
47. S. Martinez-Bartolome *et al.*, *Mol Cell Proteomics* **7**, 1135 (Jun, 2008).
48. P. Navarro *et al.*, *J Proteome Res* **13**, 1234 (Mar 7, 2014).
49. F. Garcia-Marques *et al.*, *Mol Cell Proteomics* **15**, 1740 (May, 2016).

Acknowledgements

We thank M. Calvo and G. Martín and acknowledge the use of the Advanced Optical Microscopy Facility of University of Barcelona. We are indebted to C. Ferguson and J. Rae and acknowledge the use of the Australian Microscopy & Microanalysis Research Facility at the Center for Microscopy and Microanalysis at The University of Queensland. We thank J. Murphy (Walter and Elizabeth Hall Institute of Medical Research, Melbourne, Australia) for providing the pF_TRE3G_PGK_puro construct. We are indebted to the Protein Expression Facility (University of Queensland) for valuable assistance. We thank the Australian Red Cross Blood Service for providing buffy coats for the isolation of human monocytes. Finally, we are indebted to the Citomics unit of IDIBAPS for their technical help. **Funding:** M.B. acknowledges support from 31/U/2016 from Fundació Marató de TV3. R.K. acknowledges support from an Australian Research Council Discovery Early Career Research Award (DE130100470). B.S. is supported by an Early Postdoc Mobility fellowship from the Swiss National Science Foundation (P2ZHP3_184024). M.J.S. is supported by a National Health and Medical Research Council (NHMRC) Senior Research Fellowship (APP1107914). M.S-A. was recipient of a CNIC IPP fellowship (COFUND 2014). M.M. is supported by the Instituto de Salud Carlos III (FIS PI19/01410). O.T. is founded by Amgen 2018 Competitive Grant Program. A.P., R.G.P., S.P.G. and P.B. have been supported by RGP0020/2015 from the Human Frontier Science Program (HFSP). A.P. is supported by the Ministerio de Ciencia e Innovación (MICINN, RTI2018-098593-B-I00), Fundació Marató de TV3 (31/U/2016), and the CERCA Programme/Generalitat de Catalunya. R.G.P. was supported by the NHMRC of Australia (program grant, APP1037320 and Senior Principal Research Fellowship, 569452), and the Australian Research Council Centre of Excellence in Convergent Bio-Nanoscience and Technology (CE140100036). P.T.B. is supported by Conselho Nacional de Desenvolvimento Científico e Tecnológico (CNPq) of Brazil and Fundaçao de Amparo a

Pesquisa do Estado do Rio de Janeiro (FAPERJ). M.A.P. was funded by MICINN (project grants SAF2014-51876-R and SAF2017-83130-R; and IGP-SO grant MINSEV1512-07-2016) and was a Worldwide Cancer Research Foundation grantee (# 15-0404). J.V. is supported by MICINN (BIO2015-67580-P) and from the Carlos III Institute of Health-Fondo de Investigación Sanitaria (PRB2, IPT13/0001—ISCIII-SGEFI/FEDER, ProteoRed). The CNIC is supported by the MICINN and the Pro-CNIC Foundation and is a Severo Ochoa Center of Excellence (MICINN award SEV-2015-0505). **Author contributions:** M.B., and M.S-A., contributed equally. Conceptualization, M.B., P.T.B., S.P.G., R.G.P., and A.P. Methodology, M.B., M.S-A., and A.F. Formal Analysis, M.B., R.G.P., and A.P. Investigation, M.B., M.S-A., A.F., R.K., B.S., F.D., L.M., M.M., F.M-P., O.T., A.G., R.M.T., J.E.C., C.C., N.M., and F.T. Resources and Supervision, F.L., C.E., M.A.P., M.J.S., P.T.B., S.P.G., R.G.P., and A.P. Data Curation, M.B., M.S-A., F.T., R.G.P., and A.P. Writing – Original Draft, R.G.P., and A.P. Writing – Review & Editing, M.B., and M.S-A., M.S., P.T.B., S.P.G., R.G.P., and A.P. Visualization, R.G.P., and A.P. Project Administration, P.T.B., S.P.G., R.G.P., and A.P. Funding Acquisition, P.T.B., S.P.G., R.G.P., and A.P. **Competing interests:** None. **Data and materials availability**: Mass spectrometry data have been deposited in Peptide Atlas (ID: PASS01610). Computer code#1 to measure LD-mitochondria contacts can be found at: https://zenodo.org/badge/latestdoi/280189667. Computer code#2 to quantify distribution of LD proteins can be found in: https://zenodo.org/badge/latestdoi/280200243.

Figure Legends

Fig. 1. Mammalian LDs display regulated protein-mediated antibacterial activity. (**A** and **B**) Representative hematoxylin-eosin-stained sections (left) and TEM images (right) of CTL- (A) or LPS-livers (B) (representative of N = 3). Red arrows and asterisks indicate LDs. Scale bars: 100 µm (left); and 5 µm (right). (**C**) Hepatic triacylglycerol levels (TG) in CTL- and LPS-mice (N = 5). (**D** and **E**) Hepatic LD number (D) and mean LD area (E) measured in TEM images of at least 13 random sections of CTL- or LPS-livers (combined from N = 2) (see fig. S6). (**F**) CTL- and LPS-livers were fractionated in sucrose density gradients and LDs floated onto the top fraction ("LDs"), as assessed by anti-PLIN2 immunoblotting (see fig. S1A) (representative of N = 5). (**G**) *E. coli* were incubated for 16 hours in standard medium (gray) or medium supplemented with proteins from CTL- (black)

or LPS-LDs (red bar). CFU measurements were normalized to the standard medium condition (N ≥ 7) (see fig. S1). (**H**) Unloaded (black) and OA-loaded HMDMs (red bars) were infected with *E. coli* or *Salm* for 4 hours. LD number per cell was quantified in TEM images in at least eight macrophages per condition (combined from N = 3). (**I** and **J**) Control (black) and OA-loaded HMDMs (red bars) were infected with *E. coli* (I) or *Salm* (J) and bacterial loads (CFU) determined 24 hours later (N = 5). (**K**) Control (black) and OA-loaded HMDMs (red bars) were incubated with pHrodo *E. coli* and bacterial loads measured (fluorescence units) (N = 3). Cyt D was used to inhibit phagocytosis. (**L**) Length of LD-bacteria contacts per cell was measured in TEM images of OA-loaded HMDMs infected with *E. coli* or *Salm* for 4 hours in at least 15 macrophages per condition (combined from N = 3) (see fig. S2, A to D). (**M** to **R**) Control (M, O, and P) and OA-loaded HMDMs (N and R) were infected with *E. coli* for 4 hours and analyzed in TEM images. Representative images have been colored blue (ER), red (*E. coli* interior), green (periplasm), and yellow (vacuolar membrane) (see fig. S2, E and F) (representative of N = 3). Scale bars: 2 µm (M and N); and 0.5 µm (O and R). All graphs show mean + SD; not significant (ns), * P<0.05, ** P<0.01, ***P<0.001, ****P<0.0001 in a paired t test (C to E; H to J; and L), and one-way ANOVA test (G and K).

Fig. 2. Quantitative mass spectrometry analysis of LPS-LDs.

(**A**) The figure summarizes changes in the proteome of LPS-livers (N = 3) and LPS-LDs (N = 5) when compared to CTL-livers (N = 3) or CTL-LDs (N = 4), respectively. "Identified" (gray letters) indicates identified proteins and "Regulated" (black letters) proteins significantly modified by LPS. Among modified proteins, yellow and blue circles indicate up- and downregulated proteins, respectively (tables S1 to S5). (**B**) Functional annotation enrichment analysis of proteins increasing (|ΔZq|>1.8; yellow graphs) or decreasing (|ΔZq|<minus1.8; blue graphs) on LPS-LDs when compared to CTL-LDs. Enrichment as compared to the mouse genome for each category is expressed as –log (P-value). Analyses for CTL- and LPS-livers is shown in fig. S3A. (**C**) Pie charts summarizing LPS-induced changes in bona fide LD proteins. Protein details are in tables S6 and S7 and annotated interactions in fig. S3B. (**D**) Hierarchical clustering of Zq values across replicates identifies functionally coherent protein subsets similarly regulated by LPS (threshold for cluster analysis: r>0.78). The cluster nucleated around PLIN2 is included. Five additional clusters are detailed in fig. S4A. (**E**) Gene subnetwork from IPA analysis of all identified proteins upregulated in LPS-LDs.

Fig. 3. Physical and functional uncoupling of LPS-LDs and mitochondria.
(**A**) Relative enrichment of selected proteins. Protein enrichment in LPS-LDs illustrated by a heatmap code (blue, depletion; yellow, enrichment). The Δ*Zq*, UniProt ID, ranking (tables S3 to S5), and a representative immunoblot (representative of N = 3) are indicated. (**B**) Fed-, CTL-, and LPS-livers were fractionated in sucrose gradients and LD–mitochondria co-fractionation determined by immunoblotting of ATP5D (a subunit of ATP synthase) (representative of N = 3). (**C**) Functional categories of downregulated mitochondrial proteins cofractionating with LPS-LDs are compared with the whole mitochondrial proteome (MitoCarta 2.0). (**D** and **E**) The mitochondrial content of CTL- (black) and LPS-livers (red bars) was determined by citrate synthase activity (D) and DNA copy number of COI (E, relative to GAPDH) (N = 6). (**F**) Percentage of LDs interacting with mitochondria in CTL- (black) and LPS-livers (red bars) was quantified in TEM images of at least 15 random sections per condition (combined from N = 2) (see fig. S6). (**G** and **H**) Mitochondrial beta-oxidation (G) and formation of soluble intermediates (H, ketone bodies) of lipids stored in LDs were quantified for 16 hours in primary hepatocytes left untreated (black) or treated with LPS (red bars) (N = 5). (**I**) Ketones in sera of CTL- (black) and LPS-mice (red bars) (N = 4). (**J**) Fed-, CTL-, and LPS-livers were fractionated in density gradients and PLIN5 distribution analyzed by immunoblotting (representative of N = 5). (**K**) HuH7 cells were transfected with a tagged *PLIN5*, and labeled with anti-FLAG antibodies (PLIN5), anti-TOM20 antibodies (mitochondria), and LipidTox (LDs). Contours of a representative transfected and non-transfected cell are indicated (representative of N = 3). The arrow marks a mitochondrion completely enwrapping a LD in a transfected cell. Scale bar, 20 µm. (**L**) LPS sensitive HEK293-TLR4^{+} cells transfected with a tagged *PLIN5* were loaded with OA (black) or with OA + LPS (red dots). The length of LD-mitochondria contacts per cell was measured in confocal microscopy images (see example in fig. S7, D to F) of 66 transfected cells and 470 non-transfected cells (combined from N = 3). (**M**) HEK293 cells were transfected with FLAG-tagged *PLIN3* or *PLIN5*, loaded with OA, and protein expression determined by immunoblotting (M, left). Cells were infected with *E. coli*, and bacterial loads quantified after 4 hours (M, right) (N = 4). (**N**) THP-1 cells were transduced with *PLIN5*-encoding or empty lentiviral vectors. PLIN5 expression was confirmed by immunoblotting (N, left). Transduced cells were infected with *E. coli* and bacterial loads evaluated after 8 hours (N, right) (N = 3) (see fig. S7, G to J). All graphs show mean + SD; not significant (ns), * P<0.05, ** P<0.01,

***P<0.001, in a paired t test (D, E, G to I, M and N), one-way ANOVA test (L), and two-sided Student's z test on proportions (F).

Fig. 4. LDs accumulate and utilize innate immunity proteins.

(**A** to **C**) Relative enrichment of selected proteins. Protein enrichment in LPS-LDs was evaluated as in Fig. 3. Accumulation of transfected proteins on LDs was confirmed in HuH7 cells by immunofluorescence (B) and fractionation in density gradients (C) (see fig. S8; fig. S9; fig. S10; and fig. S12). (**D** and **E**) HMDMs were transfected with a scrambled (Scr) or with a CAMP siRNA, and CAMP expression determined by qRT-PCR (D). Then, unloaded and OA-loaded HMDMs were infected with *E. coli* for 8 hours, and bacterial loads (CFU) were quantified (N = 5). (**F**) HEK293 cells were transfected with a tagged LD-*CAMP* (fig. S12) and loaded with OA. LD-CAMP was detected on LDs (LipidTox) with anti-FLAG and anti-CAMP antibodies. (**G**) HEK293 cells were transfected with LD-*CAMP* (red) or *PLIN3* (black bars), loaded with OA, and infected with the indicated bacteria for 4 hours. Bacterial loads (CFU values normalized to *PLIN3*-cells) were quantified (N ≥ 3). (**H** to **J**) LD-*CAMP*-transfected HEK293 cells were incubated in control (black) or OA containing medium (red bars). Cellular LD-CAMP levels (H) and LD accumulation (I) were assessed by immunoblotting with anti-CAMP antibodies. These cells were then infected with *E. coli* for 4 hours and bacterial loads quantified (J) (N = 7). All graphs show mean + SD; not significant (ns), * P<0.05, ** P<0.01, ***P<0.001 in a paired t test.

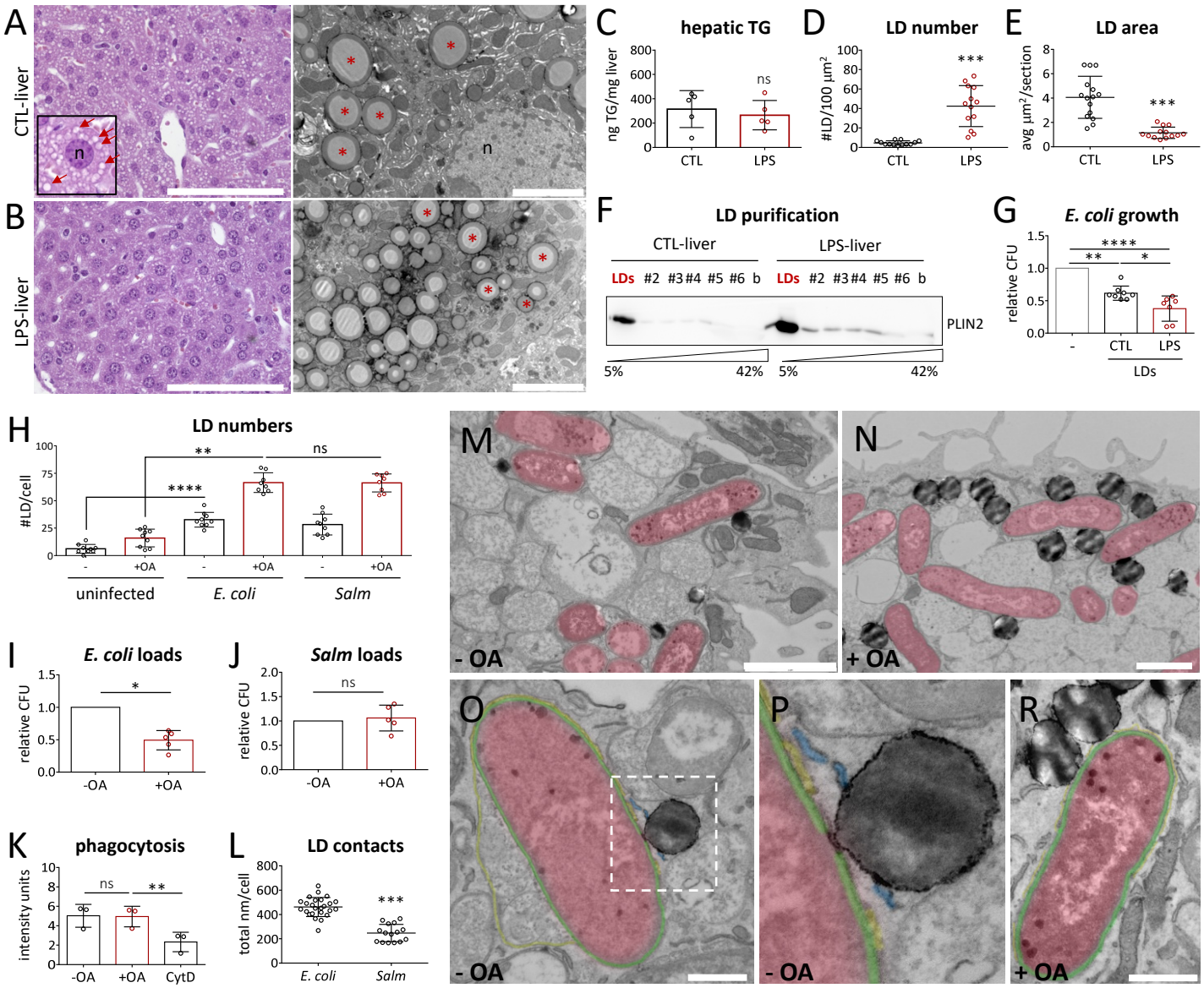
A
CTL-liver
n
n
B
LPS-liver
C
hepatic TG
ng TG/mg liver
800
600
400
200
0
ns
CTL
LPS
D
LD number
#LD/100 µm²
100
80
60
40
20
0
***
CTL
LPS
E
LD area
avg µm²/section
8
6
4
2
0
***
CTL
LPS
F
LD purification
CTL-liver
LPS-liver
LDs #2 #3 #4 #5 #6 b
LDs #2 #3 #4 #5 #6 b
PLIN2
5%
42%
5%
42%
G
E. coli growth
relative CFU
1.5
1.0
0.5
0.0
****
**
*
-
CTL
LPS
LDs
H
LD numbers
#LD/cell
100
75
50
25
0
**
ns
****
-
+OA
-
+OA
-
+OA
uninfected
E. coli
Salm
I
E. coli loads
relative CFU
1.5
1.0
0.5
0.0
*
-OA
+OA
J
Salm loads
relative CFU
2.0
1.5
1.0
0.5
0.0
ns
-OA
+OA
K
phagocytosis
intensity units
10
8
6
4
2
0
ns
**
-OA
+OA
CytD
L
LD contacts
total nm/cell
800
600
400
200
0
***
E. coli
Salm
M
- OA
N
+ OA
O
- OA
P
- OA
R
+ OA

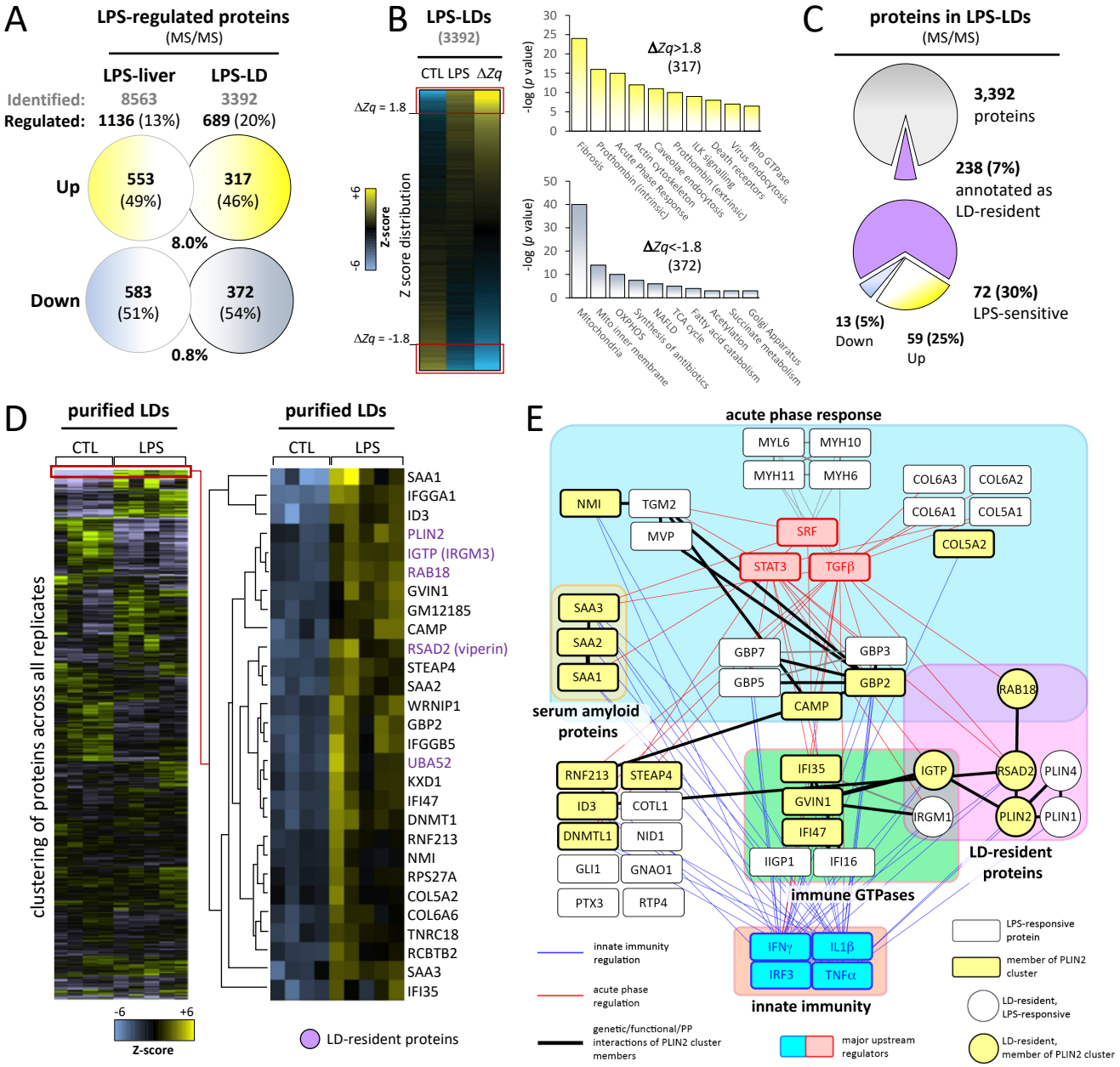
A
LPS-regulated proteins
(MS/MS)
LPS-liver
LPS-LD
Identified:
8563
3392
Regulated:
1136 (13%)
689 (20%)
Up
553
(49%)
317
(46%)
8.0%
Down
583
(51%)
372
(54%)
0.8%
B
LPS-LDs
(3392)
CTL LPS ΔZq
ΔZq = 1.8
ΔZq = -1.8
+6
-6
Z-score
Z score distribution
-log (p value)
ΔZq>1.8
(317)
Rho GTPase
Virus endocytosis
Death receptors
IL6 signalling
Prothrombin (extrinsic)
Caveolae endocytosis
Actin cytoskeleton
Acute Phase Response
Prothrombin (intrinsic)
Fibrosis
ΔZq<-1.8
(372)
Golgi Apparatus
Succinate metabolism
Acetylation
Fatty acid catabolism
TCA cycle
NAFLD
Synthesis of antibiotics
OXPHOS
Mito inner membrane
Mitochondria
C
proteins in LPS-LDs
(MS/MS)
3,392
proteins
238 (7%)
annotated as
LD-resident
72 (30%)
LPS-sensitive
13 (5%)
Down
59 (25%)
Up
D
purified LDs
CTL
LPS
clustering of proteins across all replicates
SAA1
IFGGA1
ID3
PLIN2
IGTP (IRGM3)
RAB18
GVIN1
GM12185
CAMP
RSAD2 (viperin)
STEAP4
SAA2
WRNIP1
GBP2
IFGGB5
UBA52
KXD1
IFI47
DNMT1
RNF213
NMI
RPS27A
COL5A2
COL6A6
TNRC18
RCBTB2
SAA3
IFI35
-6
+6
Z-score
LD-resident proteins
E
acute phase response
MYL6
MYH10
MYH11
MYH6
COL6A3
COL6A2
COL6A1
COL5A1
COL5A2
NMI
TGM2
MVP
SRF
STAT3
TGFβ
SAA3
SAA2
SAA1
serum amyloid
proteins
GBP7
GBP5
GBP3
GBP2
CAMP
RAB18
RNF213
STEAP4
ID3
COTL1
DNMTL1
NID1
GLI1
GNAO1
PTX3
RTP4
IFI35
GVIN1
IFI47
IIGP1
IFI16
IGTP
IRGM1
RSAD2
PLIN4
PLIN2
PLIN1
LD-resident
proteins
immune GTPases
IFNγ
IL1β
IRF3
TNFα
innate immunity
innate immunity
regulation
acute phase
regulation
genetic/functional/PP
interactions of PLIN2 cluster
members
major upstream
regulators
LPS-responsive
protein
member of PLIN2
cluster
LD-resident,
LPS-responsive
LD-resident,
member of PLIN2 cluster

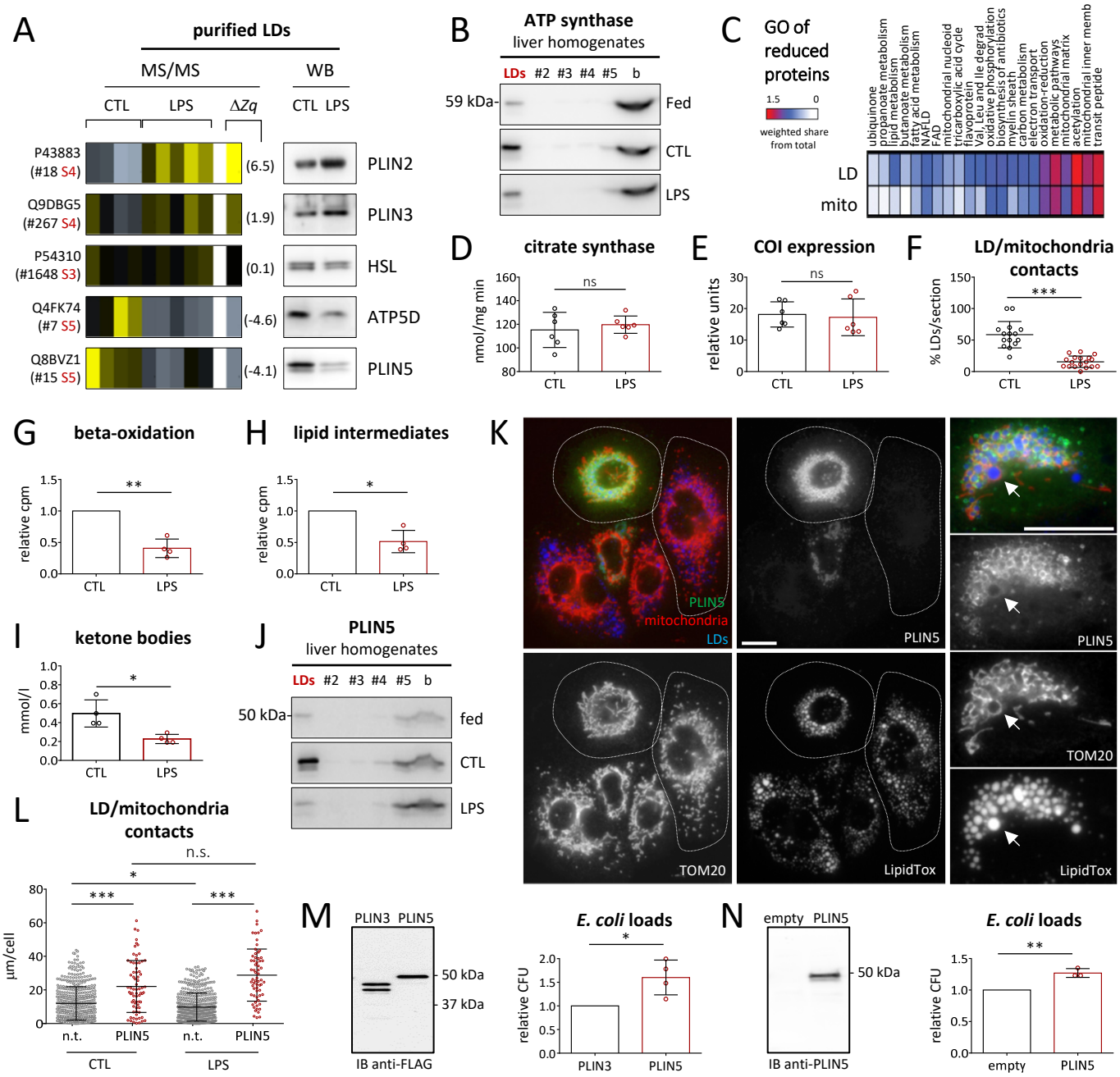
A
purified LDs
MS/MS
WB
CTL
LPS
ΔZq
CTL LPS
P43883 (#18 S4)
Q9DBG5 (#267 S4)
P54310 (#1648 S3)
Q4FK74 (#7 S5)
Q8BVZ1 (#15 S5)
(6.5)
(1.9)
(0.1)
(-4.6)
(-4.1)
PLIN2
PLIN3
HSL
ATP5D
PLIN5
B
ATP synthase
liver homogenates
LDs #2 #3 #4 #5 b
59 kDa
Fed
CTL
LPS
C
GO of reduced proteins
1.5
0
weighted share from total
ubiquinone
ubiquinate metabolism
lipid metabolism
butanoate metabolism
fatty acid metabolism
NAFLD
FAD
mitochondrial nucleoid
tricarboxylic acid cycle
flavoprotein
Val, Leu and Ile degrad
oxidative phosphorylation
biosynthesis of antibiotics
myelin sheath
carbon metabolism
electron transport
oxidoreductase
metabolic pathways
mitochondrial matrix
acetylation
mitochondrial inner memb
transit peptide
LD
mito
D
citrate synthase
nmol/mg min
ns
CTL
LPS
E
COI expression
relative units
ns
CTL
LPS
F
LD/mitochondria contacts
% LDs/section
***
CTL
LPS
G
beta-oxidation
relative cpm
**
CTL
LPS
H
lipid intermediates
relative cpm
*
CTL
LPS
I
ketone bodies
mmol/l
*
CTL
LPS
J
PLIN5
liver homogenates
LDs #2 #3 #4 #5 b
50 kDa
fed
CTL
LPS
K
PLIN5
mitochondria
LDs
PLIN5
PLIN5
TOM20
TOM20
LipidTox
LipidTox
L
LD/mitochondria contacts
n.s.
*
***
***
µm/cell
n.t.
PLIN5
n.t.
PLIN5
CTL
LPS
M
PLIN3 PLIN5
50 kDa
37 kDa
IB anti-FLAG
E. coli loads
*
relative CFU
PLIN3
PLIN5
N
empty PLIN5
50 kDa
IB anti-PLIN5
E. coli loads
**
relative CFU
empty
PLIN5

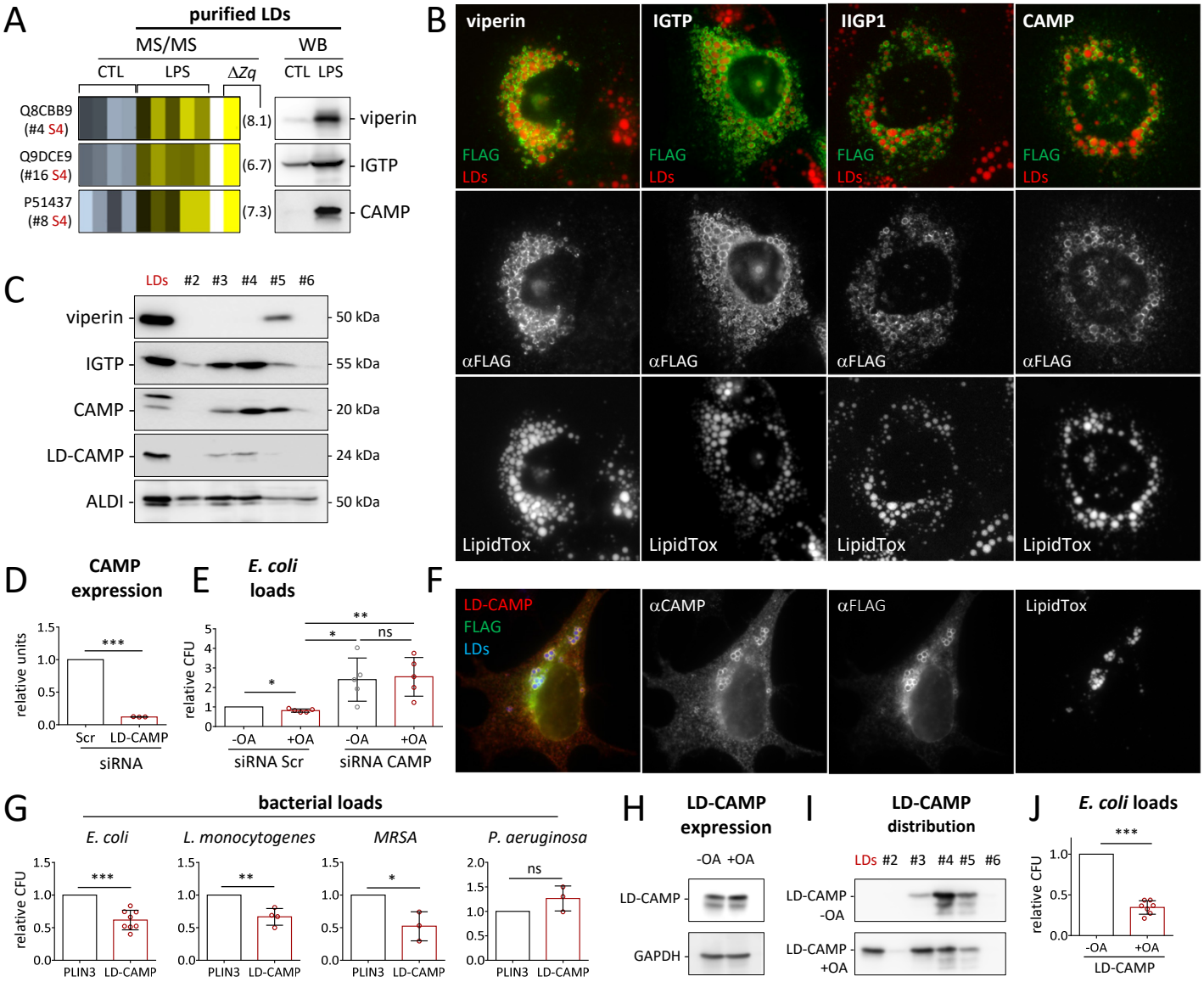
A
purified LDs
MS/MS
WB
CTL
LPS
ΔZq
CTL
LPS
Q8CBB9
(#4 S4)
Q9DCE9
(#16 S4)
P51437
(#8 S4)
(8.1)
(6.7)
(7.3)
viperin
IGTP
CAMP
B
viperin
IGTP
IIGP1
CAMP
FLAG
LDs
αFLAG
LipidTox
C
LDs #2 #3 #4 #5 #6
viperin
IGTP
CAMP
LD-CAMP
ALDI
50 kDa
55 kDa
20 kDa
24 kDa
50 kDa
D
CAMP expression
relative units
Scr
LD-CAMP
siRNA
E
E. coli loads
relative CFU
-OA
+OA
siRNA Scr
siRNA CAMP
ns
F
LD-CAMP
FLAG
LDs
αCAMP
αFLAG
LipidTox
G
bacterial loads
E. coli
L. monocytogenes
MRSA
P. aeruginosa
relative CFU
PLIN3
LD-CAMP
ns
H
LD-CAMP expression
-OA +OA
LD-CAMP
GAPDH
I
LD-CAMP distribution
LDs #2 #3 #4 #5 #6
LD-CAMP -OA
LD-CAMP +OA
J
E. coli loads
relative CFU
-OA
+OA
LD-CAMP